Am J Physiol Heart Circ Physiol 306: H270–H278, 2014.
First published November 8, 2013; doi:10.1152/ajpheart.00818.2012.

Experimental model of transthoracic, vascular-targeted, photodynamically induced myocardial infarction

Adrian Chrastina,[1] Peter Pokreisz,[2] and Jan E. Schnitzer[1]

[1]*Proteogenomics Research Institute for Systems Medicine, San Diego, California; and* [2]*Department of Cardiovascular Sciences, Catholic University of Leuven, Leuven, Belgium*

Submitted 2 November 2012; accepted in final form 6 November 2013

Chrastina A, Pokreisz P, Schnitzer JE. Experimental model of transthoracic, vascular-targeted, photodynamically induced myocardial infarction. *Am J Physiol Heart Circ Physiol* 306: H270–H278, 2014. First published November 8, 2013; doi:10.1152/ajpheart.00818.2012.—We describe a novel model of myocardial infarction (MI) in rats induced by percutaneous transthoracic low-energy laser-targeted photodynamic irradiation. The procedure does not require thoracotomy and represents a minimally invasive alternative to existing surgical models. Target cardiac area to be photodynamically irradiated was triangulated from the thoracic X-ray scans. The acute phase of MI was histopathologically characterized by the presence of extensive vascular occlusion, hemorrhage, loss of transversal striations, neutrophilic infiltration, and necrotic changes of cardiomyocytes. Consequently, damaged myocardium was replaced with fibrovascular and granulation tissue. The fibrotic scar in the infarcted area was detected by computer tomography imaging. Cardiac troponin I (cTnI), a specific marker of myocardial injury, was significantly elevated at 6 h (41 ± 6 ng/ml, $n = 4$, $P < 0.05$ vs. baseline) and returned to baseline after 72 h. Triphenyltetrazolium chloride staining revealed transmural anterolateral infarcts targeting $25 \pm 3\%$ of the left ventricle at *day 1* with a decrease to $20 \pm 3\%$ at *day 40* ($n = 6$ for each group, $P < 0.01$ vs. *day 1*). Electrocardiography (ECG) showed significant ST-segment elevation in the acute phase with subsequent development of a pathological Q wave and premature ventricular contractions in the chronic phase of MI. Vectorcardiogram analysis of spatiotemporal electrical signal transduction revealed changes in inscription direction, QRS loop morphology, and redistribution in quadrant areas. The photodynamically induced MI in $n = 51$ rats was associated with 12% total mortality. Histological findings, ECG abnormalities, and elevated cTnI levels confirmed the photosensitizer-dependent induction of MI after laser irradiation. This novel rodent model of MI might provide a platform to evaluate new diagnostic or therapeutic interventions.

myocardial ischemia; myocardial infarction; animal model; photosensitizer; CT imaging; ECG; VCG; laser

DESPITE CONSIDERABLE EFFORT and progress in the research of coronary heart disease, myocardial infarction (MI) remains the leading cause of mortality, morbidity, and disability worldwide. MI and subsequent left ventricular (LV) dysfunction and heart failure are the consequences of prolonged myocardial ischemia after coronary occlusion. MI compromises the capacity of the heart to pump blood because of the loss of contractile mass from the affected myocardium. Ultimately MI may thereby lead to sudden death or severe hemodynamic deterioration.

Small animal models (predominantly mice and rats) of cardiovascular disease provide fundamental data and indispensable tools for preclinical research of human cardiac diseases (25, 42). Rats in particular have been utilized in cardiovascular studies on imaging (53), therapy (18, 31, 59), and LV remodeling and repair (24, 51) after MI. There are several small animal models of MI, all of which require invasive surgery. Ligation of the coronary artery is the most commonly used method to induce MI. This involves exposure of the heart after thoracotomy, opening of the pericardial sac, and occlusion of the coronary artery with suture (12, 32). Although this method is frequently used, open-chest surgery on small rodents results in relatively high perioperative mortality, postoperative wound healing, and inflammatory reactions. Furthermore, the reproducibility of coronary artery ligation requires extensive surgical practice and may result in infarcts of variable size (58). The other methods, including cauterization (7) and cryoinfarction/cryoinjury (58), also require invasive surgery. Balloon occlusion (15) is minimally invasive but technically more challenging and ultimately less feasible in small rodents. Additionally, there are several methods of pharmacologically inducible MI, including isoproterenol administration (61). However, these methods have limitations in predicting the time frame of development, the location, and the actual size of MI. Therefore, a minimally invasive method resulting in sizewise reproducible, well-localized MI, without the necessity of open-chest surgery, would be of significant interest and potential benefit to this field of research.

Previously, we have reported a model of laser-targeted photosensitizer-induced lung infarction (14). Using this concept of photodynamically induced infarction, we have developed a small animal model of MI. The procedure is based on laser irradiation of the myocardium through the intact chest wall of animals, which systemically received the photosensitizer chlorin e6. On excitation by the laser, the photosensitizer mediates production of cytotoxic reactive oxygen species that subsequently lead to vascular damage and development of infarction in the irradiated area of myocardium. This methodology allows rapid and reproducible induction of MI without an invasive surgical intervention and with little to no recovery time necessary after the procedure. The presented rat model might be applied potentially to other small rodents and could serve in the preclinical development of novel diagnostic and therapeutic strategies of MI.

MATERIALS AND METHODS

Materials. Chlorin e6 [Fotolon; (2*S*-trans)-18-carboxy-20-(carboxymethyl)-13-ethyl-2,3-dihydro-3,7,12,17-tetramethyl-8-vinyl-21*H*,23*H*-porphine-2-propionic acid] was purchased from Frontier Scientific (Logan, UT). All other chemicals were received from Sigma-Aldrich (St Louis, MO).

Address for reprint requests and other correspondence: A. Chrastina, Proteogenomics Research Institute for Systems Medicine, 11107 Roselle St., San Diego, CA 92121 (e-mail: achrastina@prism-sd.org or ado_boston@yahoo.com).

Animals and experimental study design. All animal experiments were carried out in accordance with protocols approved by the Institutional Animal Care and Use Committee at the Proteogenomics Research Institute for Systems Medicine. All procedures were performed according to the *Guidelines for the Care and Use of Experimental Animals*. Fisher CDF rats (females, 170–180 g, 8–9 wk old) were purchased from Charles River Laboratories (Wilmington, MA). Animals were housed in the animal care facility in rooms maintained at +22°C under standard 12-h light-dark cycle and provided free access to pelleted 18% protein rodent diet (Harlan) and purified drinking water ad libitum.

X-ray-guided positioning of the irradiation beam and triangulation of the target site. Triangulation of the target site was performed with assistance of X-ray scans as previously described (14). Briefly, rats were anesthetized by isoflurane inhalation (1.5% vol/vol in oxygen at 1 atm, 1.0 l/min). The chest was shaved, and the surface of the left thorax was marked with X-ray contrast agent directly applied on skin in 3-mm distances apart, generating an array of fiducial marks (visible on X-ray scans) as described previously (14). Planar X-ray images were then acquired using the X-SPECT second-generation MicroSPECT imaging system (Gamma Medica, Northridge, CA) with 70 kV applied on the X-ray tube. Images were processed on a FLEX X-O system (Gamma Medica). X-ray scans allowed us to distinguish cardiac silhouette and mediastinal lines and stripes. Fiducial marks in the close proximity of the anterolateral wall of the LV were then used to guide placement of fiber-optic pipe. This triangulation minimized the possibility of peripheral pulmonary infarction. Approximately 5% of animals with signs of peripheral lung infarction during dissection were excluded from further study.

Irradiation procedure. Anesthetized animals (isoflurane, 1.5% vol/vol in oxygen at 1 atm, 1.0 l/min) were administered buprenorphine subcutaneously (0.1 mg/kg) for analgesia, and then photosensitizer (chlorine e6, 1.5 mg/kg, prepared fresh in 0.9% NaCl) was injected intravenously. Animals were positioned in supine position, and 5 min after photosensitizer injection, the target compartment located above the anterior mediastinum of the shaved chest was irradiated with a 650-nm semiconductor laser (ThinkLasers) coupled to a fiber-optic light pipe with a diameter of 1.5 mm producing a homogenous radial light pattern. The end of the optical fiber was positioned 3–4 mm from the surface of the chest with the laser beam illuminating the target area. Fifteen minutes of illumination delivered a light dose of 72 J/cm with a fluence rate of 80 mW/cm. Power flux was measured before and after irradiation of each animal by using a LaserCheck power meter (Coherent, Wilsonville, OR). For the initial experiments, the temperature was monitored with a K-type thermocouple probe (Fisher Scientific, Pittsburgh, PA) placed on the thoracic surface at the designated site of irradiation. Rats received a second dose of buprenorphine (0.1 mg/kg sc) 12 h after the irradiation procedure.

Electrocardiography. Peripheral electrocardiography (ECG) tracings were acquired from standard bipolar limb leads (lead I, lead II, and lead III) and augmented unipolar limb leads (aVL, aVF, and aVR) at a sampling rate of 0.5 kHz using the BIOPAC data acquisition system (BIOPAC, Goleta, CA) before and at designated time points after the illumination procedure under isoflurane anesthesia (1.5% vol/vol in oxygen at 1 atm, 1.0 l/min). ECG waveforms were further analyzed using AcqKnowledge (BIOPAC) and LabChart software (ADInstruments, Colorado Springs, CO).

Estimation of infarct size using triphenyltetrazolium chloride staining. Hearts were harvested from the animals at 1, 3, 6, 14, and 40 days after photodynamically induced MI. Rats were euthanized by pentobarbital sodium (Nembutal) overdose at 250 mg/kg ip, and heart tissue was removed within 30 s after death. Excised hearts were frozen at −20°C and then cut into 2-mm transverse sections from the apex to the base. Slices were then immersed in a 1% (wt/vol) solution of triphenyltetrazolium chloride (TTC) in 0.1 M phosphate buffer, pH 7.5, and incubated for 15–20 min at 37°C. The slices were then fixed in 10% formalin. Dehydrogenase activity in originally vital tissue causes deep red coloration, whereas infarcted tissue develops a pale tan color; fixation in formalin increases the contrast. Stained slices were then scanned and images analyzed for infarct size as described previously (22, 36). The infarct size (expressed as %LV) was then determined as a percentage of weight of infarction/weight of LV. The weight of infarction was estimated from the following equation: weight of infarction $= A1 \times W1 + A2 \times W2 + A3 \times W3 + \ldots + AnWn$, where A is the percent area of infarction from planimetry of a particular section n, and W is the weight of the corresponding section.

Histopathological analysis. Heart tissue samples were fixed in 4% (vol/vol) neutral-buffered formaldehyde, embedded in paraffin, cut into 5-μm-thick sections, and stained with hematoxylin-eosin. The photomicrographs were taken using a Olympus BH-2 microscope equipped with a Nikon digital camera DXM1200 (Nikon, Tokyo, Japan) and are representative of the experimental groups.

Computed tomography imaging. Computed tomography (CT) scans were acquired using the X-SPECT imaging system. CT scans were acquired using following settings: 70 kV at 350 μA and a 1 × 1 binning mode of the X-ray detector with 512 projections collected on a 360° rotation. Tomographic reconstruction has been done using a standard filtered back projection, and three-dimensional CT data sets were processed and analyzed on the AMIRA System (TGS, San Diego, CA).

Determination of cardiac troponin levels. Blood samples were collected via tail vein before and at designated time points after the photodynamically induced MI. The heparinized plasma was analyzed for concentration of rat cardiac troponin I (cTnI), which was determined in heparinized plasma using sandwich ELISA (Kamiya Biomedical, Seattle, WA) according to the manufacturer's protocol, and results are expressed as mass of circulating protein related to the plasma volume.

Statistical analyses. All results are expressed as means with corresponding standard deviation. Gaussian distribution of measured values was confirmed using Kolmogorov-Smirnov tests. To compare the infarct sizes at different time points, analysis of variance (ANOVA) was applied with consequent Dunett's test using the 1-day post-MI data as reference group. For cTnI values, ANOVA for repeated measurements was applied followed by the Bonferroni's post hoc test to evaluate the differences between respective groups, and $P < 0.05$ was considered significant. All statistical analyses were performed using the Prism program (GraphPad Software, La Jolla, CA).

RESULTS

X-ray-guided targeted laser illumination of photosensitized heart tissue induces MI. To triangulate the area to be irradiated and align laser fiber optics over the area of the LV, we performed X-ray scans of the anesthetized animals. The thoracic area was marked with X-ray contrast agent to form a matrix of reference points. The radiopaque fiducial markers were visible on X-ray scans and could be easily distinguished from high-density structures, such as thoracic bones, as well as other tissues. This array of fiducial marks facilitated triangulation and allowed positioning of the laser beam (Fig. 1, *A* and *B*) over the LV of the heart (Fig. 1*A*). Temperature measurements using a thermocouple placed at the site of irradiation showed minor fluctuations of 3 ± 1°C above the baseline temperature.

The macroscopic view of heart tissue 1 day after photodynamic laser illumination in animals that received photosensitizer showed central areas of pale pink discoloration with signs of hemorrhage (Fig. 2*G*). After 6 days, infarcted areas turned white with blood congestion at the circumference (Fig. 2*J*). Two weeks later, infarcted areas showed dense scar formation (Fig. 2*M*). Hearts of irradiated animals without photosensitizer

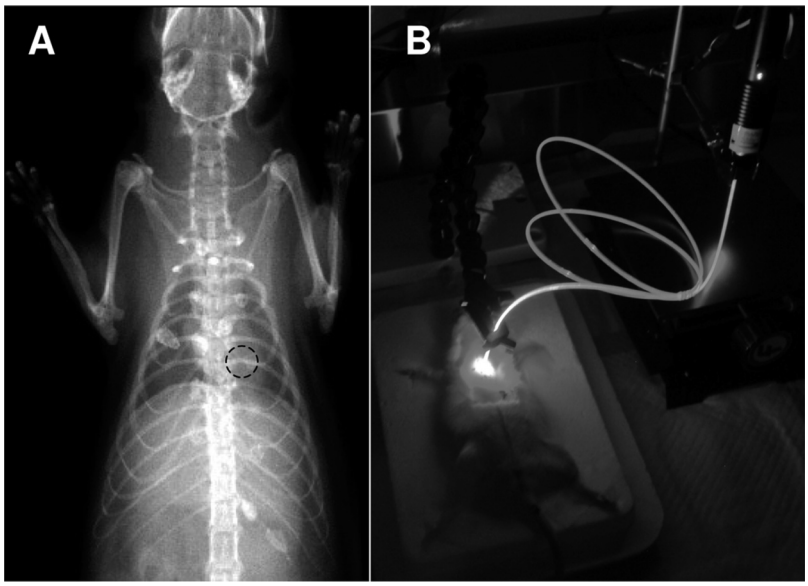

Fig. 1. X-ray image-guided positioning of laser fiber optics. *A*: X-ray scan. The thoracic area above the mediastinum was marked with fiducial marks (contrast agent) to correlate the X-ray image with the target myocardial area for laser illumination. *B*: placement of fiber-optic light pipe and transthoracic illumination procedure.

did not show myocardial damage at gross or histological levels (Fig. 2, *D–F*). Out of 51 rats that underwent photodynamically induced MI, 6 rats died within 3 days after the procedure, which indicates a total mortality rate of 12%.

Histopathological analyses reveal tissue destruction and replacement fibrosis after photodynamically induced transmural infarcts. Myocardial injury was further assessed at different time points after the photodynamic procedure by histological evaluation. Histology of heart tissue from control animals (i.e., irradiated without administration of photosensitizer) showed preserved cardiac structure and well-distinguished cardiomyocytes with intact transversal striations (Fig. 2, *E* and *F*) identical to those of untreated animals (Fig. 2, *B* and *C*). In contrast, evaluation of heart specimens harvested from irradiated animals receiving photosensitizer showed pronounced histopathological changes; 24 h after irradiation, hemorrhage and vascular occlusion were seen in the irradiated region (Fig. 2, *H* and *I*). At this time point, the infracted ventricular tissue showed myocardial degeneration with cross striations, and nuclei of cardiomyocytes were mostly lost (Fig. 2*I*). Blood capillaries and small arteries were disrupted or dilated, occluded, and filled with red blood cells hemorrhaging into the interstitial space. This was accompanied by the evident neutrophilic infiltration of the interstitium (Fig. 2*I*). Over the next 6–14 days, the affected area showed a fibrovascular response. Progressive invasion by granulation tissue took place, and this was subsequently replaced by fibrous collagenous scar tissue (Fig. 2, *K* and *L*, *N* and *O*). The brown-yellow pigmentation typical for hemosiderin deposition was occasionally present (Fig. 2, *N* and *O*). Animals that were irradiated and received photosensitizer initially showed minor scarring at the surface of irradiation site; the skin scar healed within several days. Scar formation did not occur in sham animals that were irradiated but did not receive photosensitizer. Overlying tissues above the heart appeared to be intact during the postmortem dissection but were not further analyzed for histopathological changes.

To determine the MI size, infarcted tissue and vital myocardium were demarcated using TTC staining on transversal heart sections harvested at different time points after laser illumination (Fig. 3*A*). All animals that received photosensitizer followed by irradiation showed a transmural extent of infarction targeting the anterolateral LV wall with minimal participation of the septum and right ventricle. The TTC-stained slices were also used to determine infarct size. At *day 1* after irradiation, photodynamic irradiation of animals injected with photosensitizer reproducibly induced moderate anterolateral infarcts targeting 25 ± 3% of the LV (Fig. 3*B*). The percentually expressed infarct size showed narrow variability and a moderate but statistically significant decline over 40 days to 20 ± 3% ($P < 0.01$ vs. *day 1*; Fig. 3*B*). In contrast, MI was not detectable on TTC-stained heart slices from control animals irradiated without administration of photosensitizer ($n = 6$, Fig. 3*A*, first slide).

Anterolateral infarction was associated with significant elevation of circulating cTnI after photodynamically induced MI. The plasma levels of cTnI, a marker of myocardial injury, were determined by ELISA at different time points after photodynamic infarction. Animals that received photosensitizer showed marked elevation of cTnI, 40.5 ± 5.8 ng/ml at 6 h after irradiation, significantly above baseline of the plasma collected before photodynamic irradiation (Fig. 3*C*). Consequently, cTnI levels in the plasma gradually declined with a half-life of 9.3 h within 4 days to the baseline. Plasma collected from animals before photodynamically induced infarction, as well as from irradiated animals without the photosensitizer, did not show detectable levels of cTnI (Fig. 3*C*).

Electrocardiographic findings confirm anterolateral MI. ECG electrical activity was monitored before and at designated times after photodynamic infarction. In the acute phase after irradiation procedure, the ECGs of all irradiated animals that received photosensitizer exhibited characteristic repolarization abnormalities, including ST-segment elevation in lateral leads (lead I and aVL; Fig. 4). The immediate ST elevation was followed within 3–6 h by the development of a significant Q wave (>25% of the following R wave). The representative time evolution of lead I is shown in Fig. 4. Repolarization abnormalities were attenuated, but the Q wave persisted as a sign of previous MI through all subsequent tracings (Fig. 4)

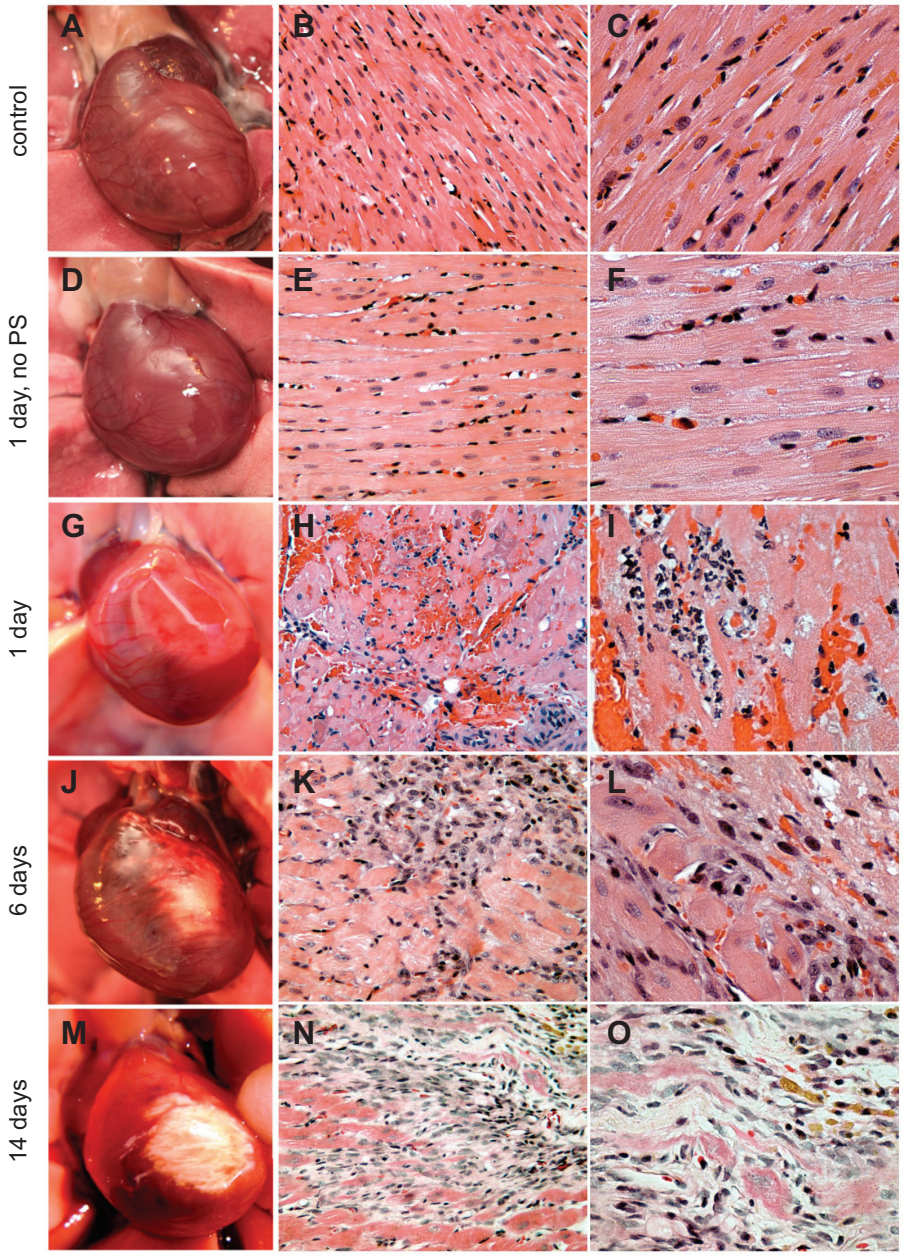

Fig. 2. Time-dependent anatomic and histopathological adaptations of irradiated heart tissue. Images at *left* (*A*, *D*, *G*, *J*, and *M*) show a macroscopic view of hearts, with corresponding hematoxylin-eosin-stained tissue sections of the irradiated area at *right* shown at different time points after laser illumination. Control hearts from an untreated animal (*A*) and from a rat 1 day after being irradiated without any administration of photosensitizer (*D*) show intact and normal anatomy. Heart specimens dissected 1 day (*G–I*), 6 days (*J–L*), and 14 days (*M–O*) after intravenous injection of photosensitizer and laser illumination demonstrate the scar formation and development of replacement fibrosis typical for myocardial infarction (MI). The presence (*C* and *F*) and loss (*I*) of transversal striations, extensive hemorrhage and vascular occlusion (*H* and *I*), neutrophil infiltration (*I*), granulation tissue (*K*, *L*, *N*, and *O*), and hemosiderin deposition (*N* and *O*) highlight the time course of the post-MI tissue rearrangement. Images represent histological findings in $n = 4$ sections per indicated time point. Magnification, ×20 (*B*, *E*, *H*, *K*, and *N*) and ×40 (*C*, *F*, *I*, *L*, and *O*). "No PS" indicates animals irradiated without photosensitizer.

in both the resolution and chronic phases. Furthermore, the ECG tracing for most of the animals (>95%) in the chronic MI phase (2–3 wk after acute MI) showed the presence of premature ventricular contractions (PVCs) with an elevated frequency of 2–4 per minute. PVCs resolved in most of the cases within 4 wk. PVCs were not detected in animals before photodynamically induced MI or before this time window.

Vectorcardiogram (VCG) recorded in frontal (*YZ*) plane showed significant distortion of QRS loop after photodynamic irradiation. Figure 5 shows VCG loops of animals before (control) and abnormally displaced VCG loops at different time points after photodynamic irradiation. Our observations indicated a significant decrease of QRS loop area, redistribution of quadrant coverage, and alteration of orientation/direction of inscription after photodynamically induced infarction. VCG recorded in the chronic phase of MI again showed the presence of PVCs. These changes supplement ECG findings and confirm spatiotemporal conductivity defects in the infarcted myocardium.

CT imaging reveals abnormal density in the infarcted tissue. To analyze the possible density changes of the infarcted myocardial tissue, thoracic CT scans were performed. Within 10 days after photodynamic infarction, we did not observe any alterations in X-ray attenuation in the infarcted area using CT images without contrast enhancement. However, 2 wk after photodynamically induced MI, we observed opacification in the irradiated area of the heart (Fig. 6, *A–C*). The opacification detected on sagittal, coronal, and axial CT slices throughout the infarcted area overlaps with the targeted site for irradiation (Fig. 1*A*) and with the scar tissue developed subsequently to the MI (Fig. 2, *M–O*).

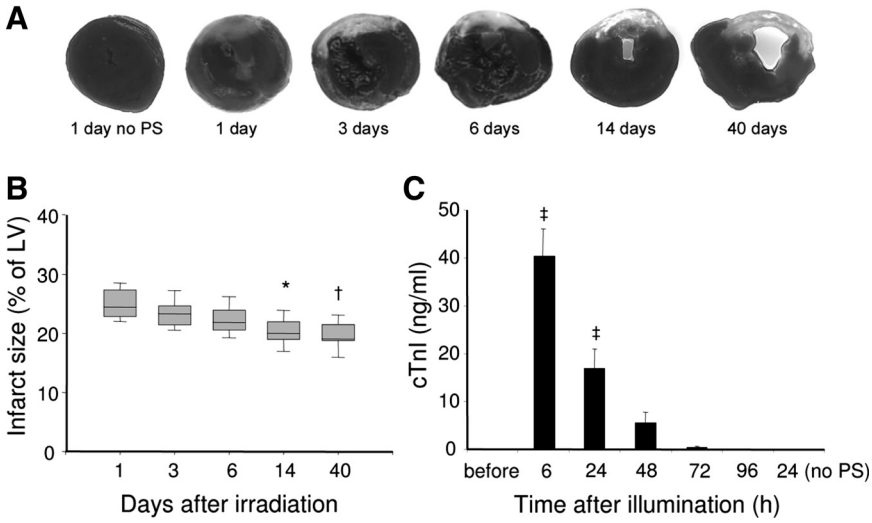

Fig. 3. Assessing infarct size and troponin I level after photodynamically induced MI. *A*: a series of triphenyltetrazolium chloride (TTC)-stained midventricular transverse tissue slices at different time points from *day 1* to *day 40* after laser illumination demonstrate time-dependent scar formation. Pale white color represents the infarcted area, whereas vital tissue stains red (dark shading). Cardiac tissue 1 day after irradiation, but without administration of photosensitizer, served as control (no PS; *A*). *B*: planimetric measurement of infarct size of TTC-stained transversal section series, expressed as a percentage of total left ventricle (LV) area, demonstrates time-dependent maturation of scar tissue. Box-and-whisker plot of infarct size ($n = 6$ per time point) as a function of time shows the minimum and maximum values, lower-upper quartiles, and median values of MI size. *$P < 0.05$; †$P < 0.01$ vs. *day 1*. *C*: time-dependent profile of plasma troponin I level after photodynamic irradiation was determined using ELISA, showing peak values 6 h after MI induction with return to baseline levels within 72 h. Data represent means ± SD ($n = 4$ for each time point). ‡$P < 0.01$ vs. baseline.

DISCUSSION

Photosensitization of tissue or light-induced, photosensitizer-mediated photocytotoxicity (photodynamic therapy, PDT) has been effectively used to ablate, eradicate, or modify tissue (8, 50). Photodynamic action is based on the excitation of a photoreactive drug (photosensitizer) by light with a wavelength tuned to the absorption band of the photosensitizer (34). The photoexcited drug transfers energy to oxygen, which generates cytotoxic and highly reactive oxygen species (45, 52). Subsequent photodestruction is mediated predominantly through vascular damage (13, 26), whereas direct phototoxicity is often limited (27). PDT has been effectively used for vascular disruption in cancer therapy (11, 35), as well as in the treatment of noncancerous pathologies, such as age-related macular degeneration (5). Photodynamically induced damage to endothelial cells and the vascular basement membrane results in thrombogenic sites in the vascular lumen and initiation of a cascade of events (including platelet aggregation, leukocyte adhesion, vasoconstriction, and increase of vascular permeability), ultimately resulting in vascular occlusion/collapse, blood flow stasis, and hemorrhage (33). In addition to cardiomyocyte necrosis, progressive granulation, and myocardial scar formation, the majority of these events were observed in the pathogenesis of MI induced by photodynamic irradiation. Within a short circulation time (5 min) following injection, the photosensitizer is not expected to extravasate into the myocardial tissue and reach significant accumulation in cardiomyocytes. Therefore, direct phototoxicity to cardiomyocytes might be marginal, and vascular occlusion is presumably the main underlying cause of myocardial ischemia and the developing MI. The vascular damage evolves into irreversible occlusion and consequently does not allow reperfusion, which represents a limitation of the presented MI model. Histological findings of MI are consistent with the concept that photosensitization and photodynamically mediated MI are not based on thermal injury. Furthermore, thermocouple-based measurements showed only a minor rise in temperature at the site of irradiation. These results confirm that the induced MI was caused specifically by a photodynamic mechanism. Irradiation of photosensitized animals produced at the surface of the illumination site just minor scarring that healed in several days. No such scarring was apparent in control (sham) animals illuminated without photosensitizer. In experiments that monitor post-MI inflammatory responses, this tissue damage has to be taken into consideration because it could add to overall inflammation.

Photodynamically induced MI does not require thoracotomy, ventilation, and suturing and consequently does not yield intra- and postoperative complications. Reports on procedures based on surgical occlusion of coronary artery include variable rodent mortality rates ranging between 13.6 and 64.6% in mice (43) and 33 and 65% in rats (29, 41), presumably because of large infarct size variability and operation procedures. However, optimization of surgical technique may lead to reduced long-term mortality 26.7% (60). Hu et al. (29) have reported 21.6% mortality in rats within 30 min after coronary artery ligation and 33% within 8-wk follow up, whereas Neubauer et al. (38) have observed 40–50% mortality within the first 24 h. In the present study we determined a total mortality rate of 12% observed within 7 wk after photodynamically induced MI. This apparent reduction may be attributed to moderate myocardial damage and less overall invasiveness of the technique, namely, avoiding extensive surgery and shortening postoperative recovery. Cardiac rupture was not observed at postmortem dissection. It is possible that this low-level mortality is caused by early arrhythmias or thrombotic events, typical for the post-MI period rather than specific to the procedural circumstances.

Despite the small heart size and rapid heart rate, this method reproducibly induced myocardial infarction in the LV of rats in a region of interest as small as 25–30 mm^2 supplied mainly by left anterior descending coronary artery. The resolution could be further improved by decreasing the diameter of optical fiber coupled to the laser and/or by using an ECG-gated output of the laser source where pulses would be overlapping with diastole.

For some studies, the small to moderate infarct size is a limitation of this model. For example, larger infarcts may be necessary to evaluate the consequences on heart failure. Otherwise well-controlled and not-so-large infarcts may be very useful to investigate many other aspects of post-MI adaptation, including resolution mechanisms, cardiac biomarkers, and therapeutic approaches. The size of the infarcted area can be potentially

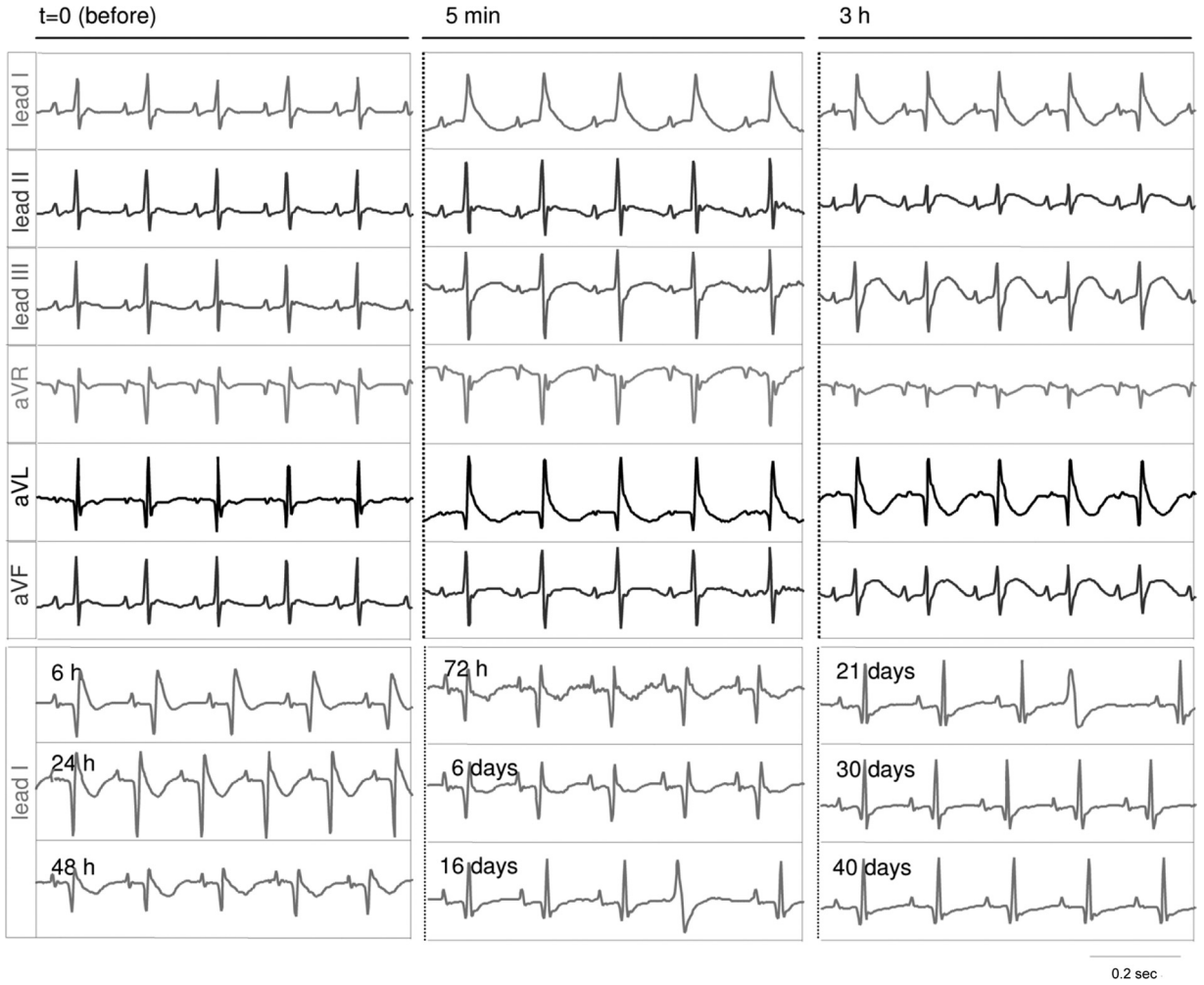

Fig. 4. Time evolution of changes in ECG activity after photodynamically induced MI. *Top*: recordings display ECG activity in standard and augmented limb leads before, 5 min, and 3 h after MI induced by photodynamic illumination. *Bottom*: waveforms show subsequent changes in lead I at indicated time points. Recordings show repolarization abnormality, including ST-segment elevation in lateral leads (leads I and aVL) in the initial phase at 5 min to 6 h after irradiation, and Q-wave development at 3 h that was persistently present until 40 days. Tracings recorded at 16 and 21 days showed the presence of premature ventricular contractions.

increased or decreased by tuning of the fiber-optic light pipe diameter and/or by changing the light dose delivered to the target area. We have tested this method on a cohort of rats with a wide range of body weight (110–300 g) and find that the most suitable body weight falls below 190 g, corresponding to an estimated depth/effective penetration of laser beam into the tissue of ~5–6 mm. If the procedure has to be done in animals with body weight above 200 g, we advise the use of a laser/photosensitizer system with longer wavelength for improved penetration of the laser beam through intercostal muscles, such as WST-09 (Tookad)/763 nm (35). Various anesthetics can be used, but isoflurane as used in our study is superior to injectable anesthesias because of rapid recovery following the irradiation procedure.

The close proximity of the lung tissue in the mediastinal region creates the possibility for the irradiation of the off target peripheral areas of the lung lobes. With the accurate triangulation of the target site using X-ray imaging, the incidence of peripheral pulmonary infarction is limited to ~5% (these animals were excluded from the study). Although the capacity for extracardiac damage can be minimized, it has to be considered depending on the exact design of the protocol and the accuracy of triangulation of the target site. We routinely use X-ray imaging as described for precise triangulation of the target area; however, in laboratories without X-ray imaging instrumentation, researchers may consider applying a less accurate determination of the irradiation site by positioning the laser fiber-optic pipe ~4 mm on the left laterally from sternum between the 7th and 8th ribs.

Beyond myocardial and lung infarction (14), this method of photodynamically induced infarction may be potentially useful to establish targeted induction of stroke as well as liver or kidney infarction. After adaptation of the light source and by application of different photosensitizers, the presented model also has translational potential for larger animals for studies requiring a small to moderate size of MI.

Histopathological findings of developing MI after photodynamic irradiation, such as loss of the cardiomyocyte's typical rod-shaped morphology, transversal striations, necrosis, and neutrophilic infiltration in the acute phase, as well as subsequent granulation and development of collagenous scar in the resolution phase, are in concordance with the well-known

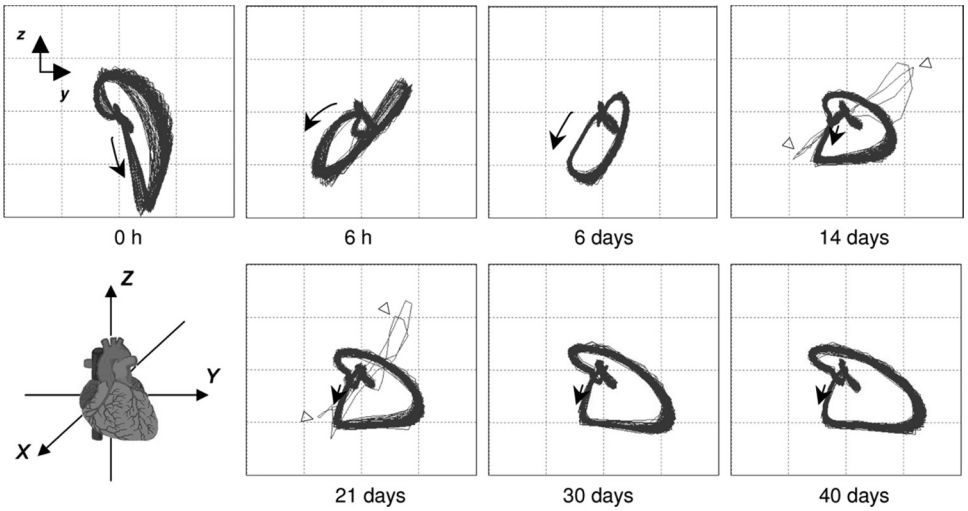

Fig. 5. Two-dimensional vectorcardiographic analysis of electrical vector in the frontal plane after photodynamically induced MI. Vectorcardiographic plots of 100 cardiac cycles recorded at different time points before and after MI revealed distortion of large QRS loop after MI. Triangles indicate premature ventricular contractions.

pathophysiology of MI (9, 21). Hemorrhage observed in the acute phase after photodynamically induced MI is a consonant consequence of increased vascular permeability (33) and severe microvascular injury, typical for acute MI (3). Decomposition of iron-containing red blood cells may lead to deposition of hemosiderin during MI (49, 57). We have also observed deposition of hemosiderin aggregates in the site of granulation.

TTC staining showed the transmural extension of the MI in all animals irradiated after photosensitizer administration. The infarct size as measured relative to the LV area declined over time modestly but with statistic significance. After MI, the LV myocardium undergoes extensive remodeling, including hypertrophy of noninfarcted myocardium and LV chamber dilatation (56). This maladaptive compensatory hypertrophy of noninfarcted LV, replacement fibrosis, and wound contracture accompanying the scar maturation may contribute to the relative decrease in infarct size. This mild decrease that we observed here in infarct size agrees with previous reports (40, 46).

The X-ray opacification that we observed in the infarcted regions 2 wk after photodynamically inducing the MI may be attributed to the presence of dense fibrotic tissue in the scar and/or to the calcification of the infarct area. It has been shown that old myocardial infarctions become calcified and detectable by non-contrast-enhanced CT (23, 47).

The electrocardiographic tracings clearly document evolution of the MI after photodynamic irradiation. Repolarization abnormality (ST-segment elevation/depression) is an indicator of acute myocardial ischemia and/or acute MI (4). The Q waves are universally recognized markers of remote MI (37). According to our observations, the ECG tracings of these depolarization and repolarization abnormalities confirm MI development after photodynamic illumination. Furthermore, the persistence of the Q wave indicates the transmural nature of the infarction (55), which we confirmed histologically by TTC staining of the tissue. Besides the presence of Q waves, PVCs were present during the chronic phase of MI. Similarly to the electrophysiological consequences of clinical MI (10), PVCs have been well documented in experimental MI models (20, 48). Often they are precursors to ventricular fibrillation (1), one of the major causes of death in patients after acute MI (44, 54). In addition to conventional ECG, two-dimensional VCG analysis proved to be superior to scalar ECG, particularly in diagnostic sensitivity of acute MI (19, 30). VCG plots clearly showed changes in orientation/direction of inscription of instantaneous heart electrical vector and abnormal QRS loop pattern.

After photodynamically induced MI, we observe an acute rise in plasma of cTnI, a standard marker of myocardial ischemia, myocardial necrosis, and acute MI (2, 16, 17, 28). The levels and time course of the peak values are consistent with the cTnI data reported by other investigators (39). According to the criteria for the diagnosis of acute MI as issued by the European Society of Cardiology and the American College of Cardiology (ESC/ACC), the rise and gradual fall in cTnI level combined with development of pathological Q waves on ECG is sufficient for the diagnosis of acute, evolving,

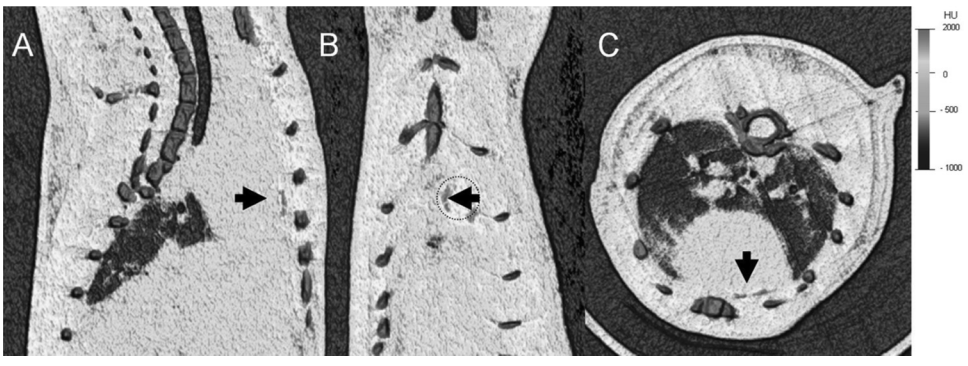

Fig. 6. CT scans of myocardial opacification in the anterior wall of the LV. Non-ECG-gated thoracic CT scans of an animal with photodynamically induced MI. Images show sagittal (*A*), coronal (*B*), and axial planes (*C*) through the thoracic cavity 12 days after irradiation. The orthoslices are displayed in the grayscale light-field mode to show differences in the tissue density. Arrows indicate the scar tissue in the infarcted myocardium. CT scans are representative of X-ray attenuation seen in animals imaged at 12 days after photodynamically induced MI ($n = 5$).

or recent MI (2, 6). Therefore, the transiently elevated cTnI and the appearance of Q waves confirm the induction and development of MI after photodynamic irradiation. These results show that focused external photodynamic irradiation can target with reasonable precision the induction and development of MI in rats.

Conclusion. The novel laser-targeted, photosensitizer-induced method reproducibly generates localized infarction in a controlled area of rat hearts using a minimally invasive procedure. This newly developed method is a noninvasive alternative to current MI models in rodents. It avoids thoracic surgery, subsequent surgical wound healing, and prolonged postoperative recovery. With only a 12% mortality rate, this photodynamically induced MI model might have significant utility for the preclinical evaluation of novel diagnostic or therapeutic strategies.

ACKNOWLEDGMENTS

We thank Alexina Wemperen (imaging facility, Proteogenomics Research Institute for Systems Medicine) for technical assistance with histology.

GRANTS

This work was supported by National Heart, Lung, and Blood Institute Grant R01 HL074063 (J. E. Schnitzer).

DISCLOSURES

No conflicts of interest, financial or otherwise, are declared by the authors.

AUTHOR CONTRIBUTIONS

A.C. conception and design of research; A.C. performed experiments; A.C. analyzed data; A.C, P.P., and J.E.S. interpreted results of experiments; A.C. prepared figures; A.C. drafted manuscript; A.C., P.P., and J.E.S. edited and revised manuscript and figures; J.E.S. approved final version of manuscript.

REFERENCES

1. **al Awadhi AH, Ravindran J, Abraham KA, Graham IM.** The prevalence and outcome of ventricular arrhythmias in acute myocardial infarction. *Ir J Med Sci* 159: 101–103, 1990.
2. **Alpert JS, Thygesen K, Antman E, Bassand JP.** Myocardial infarction redefined–a consensus document of The Joint European Society of Cardiology/American College of Cardiology Committee for the redefinition of myocardial infarction. *J Am Coll Cardiol* 36: 959–969, 2000.
3. **Asanuma T, Tanabe K, Ochiai K, Yoshitomi H, Nakamura K, Murakami Y, Sano K, Shimada T, Murakami R, Morioka S, Beppu S.** Relationship between progressive microvascular damage and intramyocardial hemorrhage in patients with reperfused anterior myocardial infarction: myocardial contrast echocardiographic study. *Circulation* 96: 448–453, 1997.
4. **Atar S, Birnbaum Y.** Ischemia-induced ST-segment elevation: classification, prognosis, and therapy. *J Electrocardiol* 38: 1–7, 2005.
5. **Augustin AJ, Scholl S, Kirchhof J.** Treatment of neovascular age-related macular degeneration: current therapies. *Clin Ophthalmol* 3: 175–182, 2009.
6. **Babuin L, Jaffe AS.** Troponin: the biomarker of choice for the detection of cardiac injury. *CMAJ* 173: 1191–1202, 2005.
7. **Brooks WW, Garibaldi BA, Conrad CH.** Myocardial injury in the mouse induced by transthoracic cauterization. *Lab Anim Sci* 48: 374–378, 1998.
8. **Brown SB, Brown EA, Walker I.** The present and future role of photodynamic therapy in cancer treatment. *Lancet Oncol* 5: 497–508, 2004.
9. **Burke AP, Virmani R.** Pathophysiology of acute myocardial infarction. *Med Clin North Am* 91: 553–572; ix, 2007.
10. **Bussmann WD, Micke G, Hildenbrand R, Klepzig H Jr.** Captopril in acute myocardial infarction: beneficial effects on infarct size and arrhythmias. *Clin Cardiol* 18: 465–470, 1995.
11. **Byrne AT, O'Connor AE, Hall M, Murtagh J, O'Neill K, Curran KM, Mongrain K, Rousseau JA, Lecomte R, McGee S, Callanan JJ, O'Shea DF, Gallagher WM.** Vascular-targeted photodynamic therapy with BF2-chelated tetraaryl-azadipyrromethene agents: a multi-modality molecular imaging approach to therapeutic assessment. *Br J Cancer* 101: 1565–1573, 2009.
12. **Camilleri JP, Joseph D, Fabiani JN, Amat D, Gueniot C, Gorny P, Barres D, Deloche A.** Experimental myocardial infarction in the rat as a quantitative model for the study of anti-ischemic interventions. *Pathol Res Pract* 172: 42–52, 1981.
13. **Chen B, Pogue BW, Hoopes PJ, Hasan T.** Vascular and cellular targeting for photodynamic therapy. *Crit Rev Eukaryot Gene Expr* 16: 279–305, 2006.
14. **Chrastina A, Schnitzer JE.** Laser-targeted photosensitizer-induced lung injury: noninvasive rat model of pulmonary infarction. *Exp Lung Res* 38: 1–8, 2012.
15. **Cohen MV, Yang XM, Liu Y, Snell KS, Downey JM.** A new animal model of controlled coronary artery occlusion in conscious rabbits. *Cardiovasc Res* 28: 61–65, 1994.
16. **Collinson PO, Gaze DC.** Biomarkers of cardiovascular damage and dysfunction–an overview. *Heart Lung Circ* 16, *Suppl* 3: S71–S82, 2007.
17. **Cummins P, Perry SV.** Troponin I from human skeletal and cardiac muscles. *Biochem J* 171: 251–259, 1978.
18. **Das H, George JC, Joseph M, Das M, Abdulhameed N, Blitz A, Khan M, Sakthivel R, Mao HQ, Hoit BD, Kuppusamy P, Pompili VJ.** Stem cell therapy with overexpressed VEGF and PDGF genes improves cardiac function in a rat infarct model. *PLoS One* 4: e7325, 2009.
19. **Dehnavi AR, Farahabadi I, Rabbani H, Farahabadi A, Mahjoob MP, Dehnavi NR.** Detection and classification of cardiac ischemia using vectorcardiogram signal via neural network. *J Res Med Sci* 16: 136–142, 2011.
20. **Epstein SE, Beiser GD, Rosing DR, Talano JV, Karsh RB.** Experimental acute myocardial infarction. Characterization and treatment of the malignant premature ventricular contraction. *Circulation* 47: 446–454, 1973.
21. **Fishbein MC, Maclean D, Maroko PR.** The histopathologic evolution of myocardial infarction. *Chest* 73: 843–849, 1978.
22. **Fishbein MC, Meerbaum S, Rit J, Lando U, Kanmatsuse K, Mercier JC, Corday E, Ganz W.** Early phase acute myocardial infarct size quantification: validation of the triphenyl tetrazolium chloride tissue enzyme staining technique. *Am Heart J* 101: 593–600, 1981.
23. **Gowda RM, Boxt LM.** Calcifications of the heart. *Radiol Clin North Am* 42: 603–617, vi–vii, 2004.
24. **Gu HJ, Gao CB, Gong JL, Li XJ, Sun B, Li XN.** Comparative proteomic analysis in left ventricular remodeling following myocardial infarction in rats. *Biomed Environ Sci* 25: 117–123, 2012.
25. **Hasenfuss G.** Animal models of human cardiovascular disease, heart failure and hypertrophy. *Cardiovasc Res* 39: 60–76, 1998.
26. **He C, Agharkar P, Chen B.** Intravital microscopic analysis of vascular perfusion and macromolecule extravasation after photodynamic vascular targeting therapy. *Pharm Res* 25: 1873–1880, 2008.
27. **Henderson BW, Dougherty TJ.** How does photodynamic therapy work? *Photochem Photobiol* 55: 145–157, 1992.
28. **Howie-Esquivel J, White M.** Biomarkers in acute cardiovascular disease. *J Cardiovasc Nurs* 23: 124–131, 2008.
29. **Hu K, Naumann A, Fraccarollo D, Gaudron P, Kaden JJ, Neubauer S, Ertl G.** Heart rate reduction by zatebradine reduces infarct size and mortality but promotes remodeling in rats with experimental myocardial infarction. *Am J Physiol Heart Circ Physiol* 286: H1281–H1288, 2004.
30. **Hurd HP 2nd, Starling MR, Crawford MH, Dlabal PW, O'Rourke RA.** Comparative accuracy of electrocardiographic and vectorcardiographic criteria for inferior myocardial infarction. *Circulation* 63: 1025–1029, 1981.
31. **Imanishi Y, Saito A, Komoda H, Kitagawa-Sakakida S, Miyagawa S, Kondoh H, Ichikawa H, Sawa Y.** Allogenic mesenchymal stem cell transplantation has a therapeutic effect in acute myocardial infarction in rats. *J Mol Cell Cardiol* 44: 662–671, 2008.
32. **Johns TN, Olson BJ.** Experimental myocardial infarction. I. A method of coronary occlusion in small animals. *Ann Surg* 140: 675–682, 1954.
33. **Krammer B.** Vascular effects of photodynamic therapy. *Anticancer Res* 21: 4271–4277, 2001.
34. **MacDonald IJ, Dougherty TJ.** Basic principles of photodynamic therapy. *J Porphy Phthalocyanines* 5: 105–129, 2001.
35. **Madar-Balakirski N, Tempel-Brami C, Kalchenko V, Brenner O, Varon D, Scherz A, Salomon Y.** Permanent occlusion of feeding arteries

and draining veins in solid mouse tumors by vascular targeted photodynamic therapy (VTP) with Tookad. *PLoS One* 5: e10282, 2010.
36. **Michael LH, Entman ML, Hartley CJ, Youker KA, Zhu J, Hall SR, Hawkins HK, Berens K, Ballantyne CM.** Myocardial ischemia and reperfusion: a murine model. *Am J Physiol Heart Circ Physiol* 269: H2147–H2154, 1995.
37. **Michael MA, El Masry H, Khan BR, Das MK.** Electrocardiographic signs of remote myocardial infarction. *Prog Cardiovasc Dis* 50: 198–208, 2007.
38. **Neubauer S, Horn M, Naumann A, Tian R, Hu K, Laser M, Friedrich J, Gaudron P, Schnackerz K, Ingwall JS, Ertl G.** Impairment of energy metabolism in intact residual myocardium of rat hearts with chronic myocardial infarction. *J Clin Invest* 95: 1092–1100, 1995.
39. **O'Brien PJ, Smith DE, Knechtel TJ, Marchak MA, Pruimboom-Brees I, Brees DJ, Spratt DP, Archer FJ, Butler P, Potter AN, Provost JP, Richard J, Snyder PA, Reagan WJ.** Cardiac troponin I is a sensitive, specific biomarker of cardiac injury in laboratory animals. *Lab Anim* 40: 153–171, 2006.
40. **Ojha N, Roy S, Radtke J, Simonetti O, Gnyawali S, Zweier JL, Kuppusamy P, Sen CK.** Characterization of the structural and functional changes in the myocardium following focal ischemia-reperfusion injury. *Am J Physiol Heart Circ Physiol* 294: H2435–H2443, 2008.
41. **Opitz CF, Mitchell GF, Pfeffer MA, Pfeffer JM.** Arrhythmias and death after coronary artery occlusion in the rat. Continuous telemetric ECG monitoring in conscious, untethered rats. *Circulation* 92: 253–261, 1995.
42. **Ou L, Li W, Liu Y, Zhang Y, Jie S, Kong D, Steinhoff G, Ma N.** Animal models of cardiac disease and stem cell therapy. *Open Cardiovasc Med J* 4: 231–239, 2010.
43. **Ovsepyan AA, Panchenkov DN, Prokhortchouk EB, Telegin GB, Zhigalova NA, Golubev EP, Sviridova TE, Matskeplishvili ST, Skryabin KG, Buziashvili UI.** Modeling myocardial infarction in mice: methodology, monitoring, pathomorphology. *Acta Naturae* 3: 107–115, 2011.
44. **Pashos CL, Newhouse JP, McNeil BJ.** Temporal changes in the care and outcomes of elderly patients with acute myocardial infarction, 1987 through 1990. *JAMA* 270: 1832–1836, 1993.
45. **Plaetzer K, Krammer B, Berlanda J, Berr F, Kiesslich T.** Photophysics and photochemistry of photodynamic therapy: fundamental aspects. *Lasers Med Sci* 24: 259–268, 2009.
46. **Pokorney SD, Rodriguez JF, Ortiz JT, Lee DC, Bonow RO, Wu E.** Infarct healing is a dynamic process following acute myocardial infarction. *J Cardiovasc Magn Reson* 14: 62, 2012.
47. **Raj V, Karunasaagarar K, Rudd JH, Screaton N, Gopalan D.** Complications of myocardial infarction on multidetector-row computed tomography of chest. *Clin Radiol* 65: 930–936, 2010.
48. **Ren B, Lukas A, Shao Q, Guo M, Takeda N, Aitken RM, Dhalla NS.** Electrocardiographic changes and mortality due to myocardial infarction in rats with or without imidapril treatment. *J Cardiovasc Pharmacol Ther* 3: 11–22, 1998.
49. **Rigol M, Solanes N, Roque M, Farre J, Batlle M, Roura S, Bellera N, Prat-Vidal C, Sionis A, Ramirez J, Sitges M, Sanz G, Bayes-Genis A, Heras M.** Hemosiderin deposits confounds tracking of iron-oxide-labeled stem cells: an experimental study. *Transplant Proc* 40: 3619–3622, 2008.
50. **Sanchez A, Reza M, Blasco JA, Callejo D.** Effectiveness, safety, and cost-effectiveness of photodynamic therapy in Barrett's esophagus: a systematic review. *Dis Esophagus* 23: 633–640, 2010.
51. **Sarapultsev P, Chupakhin O, Sarapultsev A, Rantsev M, Sidorova L, Medvedeva S, Danilova I.** New insights in to the treatment of myocardial infarction. *Int J Exp Pathol* 93: 18–23, 2012.
52. **Schmidt R.** Photosensitized generation of singlet oxygen. *Photochem Photobiol* 82: 1161–1177, 2006.
53. **Sherif HM, Saraste A, Nekolla SG, Weidl E, Reder S, Tapfer A, Rudelius M, Higuchi T, Botnar RM, Wester HJ, Schwaiger M.** Molecular imaging of early alphavbeta3 integrin expression predicts long-term left-ventricle remodeling after myocardial infarction in rats. *J Nucl Med* 53: 318–323, 2012.
54. **Solomon SD, Zelenkofske S, McMurray JJ, Finn PV, Velazquez E, Ertl G, Harsanyi A, Rouleau JL, Maggioni A, Kober L, White H, Van de Werf F, Pieper K, Califf RM, Pfeffer MA.** Sudden death in patients with myocardial infarction and left ventricular dysfunction, heart failure, or both. *N Engl J Med* 352: 2581–2588, 2005.
55. **Sullivan W, Vlodaver Z, Tuna N, Long L, Edwards JE.** Correlation of electrocardiographic and pathologic findings in healed myocardial infarction. *Am J Cardiol* 42: 724–732, 1978.
56. **Sutton MG, Sharpe N.** Left ventricular remodeling after myocardial infarction: pathophysiology and therapy. *Circulation* 101: 2981–2988, 2000.
57. **van den Bos EJ, Baks T, Moelker AD, Kerver W, van Geuns RJ, van der Giessen WJ, Duncker DJ, Wielopolski PA.** Magnetic resonance imaging of haemorrhage within reperfused myocardial infarcts: possible interference with iron oxide-labelled cell tracking? *Eur Heart J* 27: 1620–1626, 2006.
58. **van den Bos EJ, Mees BM, de Waard MC, de Crom R, Duncker DJ.** A novel model of cryoinjury-induced myocardial infarction in the mouse: a comparison with coronary artery ligation. *Am J Physiol Heart Circ Physiol* 289: H1291–H1300, 2005.
59. **Watanabe R, Ogawa M, Suzuki J, Hirata Y, Nagai R, Isobe M.** A comparison between imidapril and ramipril on attenuation of ventricular remodeling after myocardial infarction. *J Cardiovasc Pharmacol* 59: 323–330, 2012.
60. **Ye J, Yang L, Sethi R, Copps J, Ramjiawan B, Summers R, Deslauriers R.** A new technique of coronary artery ligation: experimental myocardial infarction in rats in vivo with reduced mortality. *Mol Cell Biochem* 176: 227–233, 1997.
61. **Zbinden G, Bagdon RE.** Isoproterenol-induced heart necrosis, an experimental model for the study of angina pectoris and myocardial infarct. *Rev Can Biol* 22: 257–263, 1963.